

Minimizing inter-channel cross-phase modulation with optical phase conjugation in asymmetric fibre links

GRAHAM D. HESKETH* AND PERIKLIS PETROPOULOS

Optoelectronics Research Centre University of Southampton, Highfield, Southampton, Hampshire, SO17 1BJ, UK

*G.Hesketh@soton.ac.uk

Abstract: Using analytic and numerical modelling of fibre transmission systems that employ optical phase conjugation (OPC), we show inter-channel cross-phase modulation depends on the integrated square error between nonlinear profiles before and after OPC and that arranging amplifiers and tuning power levels is crucial to minimizing noise. We derive modulation transparent formulas for phase noise and optimal power settings. Examples are shown for 16 and 64 quadrature amplitude modulation.

© 2016 Optical Society of America

OCIS codes: (190.4223) Nonlinear wave mixing; (190.5040) Phase conjugation; (200.6015) Signal regeneration.

References and links

1. A. Yariv, D. Fekete, and D. M. Pepper, "Compensation for channel dispersion by nonlinear optical phase conjugation," *Opt. Lett.* **4**, 52–54 (1979)
2. R. M. Jopson, A. H. Gnauck, R. M. Derosier, "Compensation of fibre chromatic dispersion by spectral inversion," *Electron. Lett.* , **29**(7), 576–578 (1993)
3. R. A. Fisher, B. R. Suydam, and D. Yevick, "Optical phase conjugation for time-domain undoing of dispersive self-phase-modulation effects," *Opt. Lett.* **8**(12), 611–613 (1983)
4. X. Liu, Y. Qiao, and Y. Ji, "Reduction of the fiber nonlinearity impairment using optical phase conjugation in 40 Gb/s CO-OFDM systems," *Opt. Commun.* **283**(13), 2749–2753 (2010)
5. L. B. Du, M. M. Morshed, and A. J. Lowery, "Fiber nonlinearity compensation for OFDM superchannels using optical phase conjugation," *Opt. Express*, **20**(18), 19921–19927 (2012)
6. A. D. Ellis, M. E. McCarthy, M. A. Z. Al-Khateeb, and S. Sygletos, "Capacity limits of systems employing multiple optical phase conjugators," *Opt. Express* **12**(16), 20381–20393 (2015)
7. S. Watanabe, S. Takeda, G. Ishikawa, H. Ooi, J. G. Nielsen, and C. Sonne, "Simultaneous wavelength conversion and optical phase conjugation of 200 Gb/s (5x40Gb/s) WDM signal using a highly nonlinear fiber four-wave mixer," in, *Proc. European Conference on Optical Communication (ECOC '97)*, (1997)
8. S. Watanabe and T. Chikama, "Cancellation of four-wave mixing in multichannel fibre transmission by midway optical phase conjugation," *Electron. Lett.* **30**(14), 1156–1157 (1994)
9. S. L. Jansen, D. van den Borne, B. Spinnler, S. Calabro, H. Suche, P. M. Krummrich, W. Sohler, G. D. Khoe, and H. de Waardt, "Optical phase conjugation for ultra long-haul phase-shift-keyed transmission," *J. Lightwave Technol.*, **24**(1), 54–64 (2006)
10. P. Martelli, P. Boffi, M. Ferrario, L. Marazzi, P. Parolari, R. Siano, V. Pusino, P. Minzioni, I. Cristiani, C. Langrock, M. M. Fejer, M. Martinelli, and V. Degiorgio, "All-optical wavelength conversion of a 100-Gb/s polarization-multiplexed signal," *Opt. Express* **17**(20), 17758–17763 (2009)
11. S. Yoshima, Y. Sun, K. Bottrill, F. Parmigiani, P. Petropoulos, and D. J. Richardson, "Nonlinearity mitigation through optical phase conjugation in a deployed fibre link with full bandwidth utilization," in, *Proc. European Conference on Optical Communication (ECOC '15)*, Valencia, ES (2015)
12. D. Vukovic, J. Schröder, F. Da Ros, L. B. Du, C. J. Chae, D. Choi, M. D. Pelusi, and C. Peucheret, "Multichannel nonlinear distortion compensation using optical phase conjugation in a silicon nanowire," *Opt. Express* **23**, 3640–3646 (2015)
13. F. Da Ros, I. Sackey, M. Jazayerifar, T. Richter, R. Elschner, C. Meuer, M. Nolle, L. Molle, K. Petermann, J. K. Fischer, C. Schubert, C. Peucheret, "Optical phase conjugation for nonlinearity compensation in WDM PDM 16-QAM transmission over dispersion-compensated and dispersion-uncompensated links," in *Summer Topicals Meeting Series (SUM)*, 72–73(2015)
14. S. Yoshima, Z. Liu, Y. Sun, K. Bottrill, F. Parmigiani, P. Petropoulos and D. Richardson, "Nonlinearity Mitigation for Multi-channel 64-QAM Signals in a Deployed Fiber Link through Optical Phase Conjugation," *OFC 2016 - Conference on Optical Fiber Communications Anaheim, CA 20–24* (2016)

15. I. Phillips, M. Tan, M. F. Stephens, M. McCarthy, E. Giacomidis, S. Sygletos, P. Rosa, S. Fabbri, S. T. Le, T. Kanesan, S. K. Turitsyn, N. J. Doran, P. Harper, and A. D. Ellis, "Exceeding the Nonlinear-Shannon Limit using Raman Laser Based Amplification and Optical Phase Conjugation," in *Optical Fiber Communication Conference, OSA Technical Digest* (online) (Optical Society of America, 2014), paper M3C.1.
16. P. Rosa, S. T. Le, G. Rizzelli, M. Tan, and J. D. Ania-Castañón, "Signal power asymmetry optimisation for optical phase conjugation using Raman amplification," *Opt. Express* **23**, 31772–31778 (2015)
17. K. Solis-Trapala, M. Pelusi, H. N. Tan, T. Inoue and S. Namiki, "Optimized WDM Transmission Impairment Mitigation by Multiple Phase Conjugations," *J. Lightwave Technol.*, **34**(2), 431–440 (2016)
18. H. Wei and D. V. Plant, "Simultaneous nonlinearity suppression and wide-band dispersion compensation using optical phase conjugation," *Opt. Express* **12**, 1938–1958 (2004)
19. S. Kumar and L. Liu, "Reduction of nonlinear phase noise using optical phase conjugation in quasi-linear optical transmission systems," *Opt. Express* **15**, 2166–2177 (2007)
20. P. Minzioni and A. Schiffrini, "Unifying theory of compensation techniques for intrachannel nonlinear effects," *Opt. Express* **13**, 8460–8468 (2005)
21. M. Shtaif, "Analytical description of cross-phase modulation in dispersive optical fibers," *Opt. Lett.* **23**, 1191–1193 (1998)
22. P. P. Mitra and J. B. Stark, "Nonlinear limits to the information capacity of optical fibre communications," *Nature* **411**, 1027–1030 (2001)
23. V. Tavassoli and T. E. Darcie, "Probability based modeling of cross phase modulation in 16-QAM dispersion compensated coherent systems," *Opt. Express* **19**, 13334–13342 (2011)
24. G. L. Woods, P. Papaparaskeva, M. Shtaif, I. Brener and D. A. Pitt, "Reduction of cross-phase modulation-induced impairments in long-haul WDM telecommunication systems via spectral inversion," *IEEE Photon. Technol. Lett.*, **16**(2), 677–679 (2004).
25. M. W. Maeda, W. B. Sessa, W. I. Way, A. Yi-Yan, L. Curtis, R. Spicer and R. I. Laming, "The effect of four-wave mixing in fibers on optical frequency-division multiplexed systems," *J. Lightwave Technol.* **8**(9), 1402–1408 (1990).

1. Introduction

Optical phase conjugation (OPC) is a means to optically reverse detrimental dispersive [1, 2] and nonlinear [3–5] effects in fibre optic communications, thereby enabling an increase in network information capacity [6]. The mid-span OPC element typically involves a four-wave mixing (FWM) process between a communications signal and a strong frequency offset pump in a nonlinear element [2, 7], which reproduces a phase-conjugated copy of each channel at a frequency that is spectrally inverted about the pump. The conjugated copy then propagates the remainder of the link, undoing detrimental transmission effects suffered prior to OPC. OPC is modulation format transparent, optical in nature, well suited to high bit rates and the FWM process can conjugate many channels in the same nonlinear element [8, 9]. It has also recently been shown to improve signal quality in polarization multiplexed [10] and coherent orthogonal frequency division multiplexed (CO-OFDM) signals [4, 5]. To date, transmission experiments have demonstrated improvements in Q factor of a few dB over several hundred km links using OPC in few channel wavelength division multiplexed (WDM) systems with a variety of modulation formats [11–14].

To effectively cancel nonlinearity using OPC in the absence of dispersion compensating fibre (DCF), requires either the unnatural opposition in signs for the gain/loss in spans either side of the OPC, or a power profile that is constant with respect to propagation, possibly supplied by distributed Raman amplification [15–17]. If however, pairs of DCFs and standard single-mode fibres (SMFs) are arranged in a translation symmetric fashion about an OPC such that the order of the DCF and SMF is reversed in each pair, the system requires the same sign for the loss in all fibres as naturally occurs [18] and this is the set-up considered herein.

Much theoretical work has explored OPC by treating nonlinear effects perturbatively. Results have shown that pairs of fibres with zero net dispersion separated by an OPC device are able to cancel each other's nonlinearity up to the first perturbation order and fibre parameter scaling laws have been derived that relate dispersive, nonlinear and loss parameters in the SMFs and DCFs for optimization at the leading order [18]. Expressions for the nonlinear phase noise that results from an interaction between ASE from amplifiers and the fibre nonlinearity in an OPC

system have also been derived [19]. As well as perturbative analysis, graphical methods of OPC optimization have also been explored [20]. However, neither, the exact parameter scaling laws nor the graphical optimization tools provide much analytic investigation of OPC set-ups with non-ideal fibre parameter scaling laws and their effect on nonlinear phase noise. It is also possible that perturbative analysis may also break down as one pushes to ever higher power to utilize the nonlinear cancellation and improve signal to noise ratio.

Herein, we focus on the mitigation of inter-channel XPM. In a simplified analytic model of the channel propagation [21–23] which is not perturbative in nonlinearity, we employ statistical analysis to derive the XPM noise variance. We believe that our analysis is the first analytic investigation to explicitly examine inter-channel XPM effects in OPC although signal quality improvements have been shown in numerical simulations [24]. Inter-channel XPM effects are increasingly dominant in higher level amplitude modulation formats, which are receiving much attention in recent experimental investigations involving 16 QAM [11, 12] and 64 QAM [14]. We show that XPM noise is directly proportional to the *integrated square error* in the asymmetric nonlinear profile. Understanding this, enables one to predict noise mitigation and helps to optimize set-ups by arranging amplifiers and tuning power levels. By doing so, we show that OPC enables very good cancellation of XPM even in the setting of non-ideal fibre parameter scaling laws which is often the scenario encountered with standard issue SMF and DCF.

The layout of this paper is as follows. In section 2 we present the model of inter-channel XPM in WDM which is based predominantly on models in the literature [21–23] and we derive phase noise variance. In section 3 we generalise this to incorporate an SMF followed by a fully compensating DCF, to our knowledge this generalisation does not exist in the literature. Crucially, we further generalise the analysis to incorporate OPC in sections 4 and 5, derive analytic formulas for the inter-channel XPM noise variance and discuss how to minimize this via amplifier arrangements and the tuning of power levels. In section 4 we analyse an arrangement with amplifiers before every fibre, while in 5 we only consider an amplifier at the very start of the link and immediately after the OPC. In sections 4 and 5 we show our optimization method can reduce phase noise standard deviation and we include examples with 16-QAM. Finally, in section 6 we demonstrate performance improvement with our optimization technique using bit error rate simulations of 64-QAM.

2. Phase noise model

Throughout, we refer to (1) as the field model as it describes the total scalar complex electric field envelope A travelling in the fibre with propagation constant $\beta(\omega) = \beta_2\omega^2/2 + \beta_3\omega^3/6$:

$$\frac{\partial}{\partial z}A(z, t) = \left[-\frac{\alpha}{2} - \frac{i\beta_2}{2} \frac{\partial^2}{\partial t^2} + \frac{\beta_3}{6} \frac{\partial^3}{\partial t^3} + i\gamma |A(z, t)|^2 \right] A(z, t) \quad (1)$$

where z is the distance along the fibre, t is time in the reference frame of the envelope, α is the fibre loss, β_2 and β_3 are the fibre coefficients of second and third order dispersion respectively, and γ is the fibre nonlinearity. We refer to (2) as the channel model as it describes the complex electric field a_n in the n^{th} frequency channel and is obtained from (1) through the substitution $A(z, t) = \sum_n a_n(z, t) e^{-in\Delta\omega t}$ where $\Delta\omega$ is the channel frequency separation, the sum runs over all channels and:

$$\frac{\partial}{\partial z}a_n(z, t) = \left[-\frac{\alpha}{2} + i \sum_{l=0}^3 \frac{i^l \beta_{n,l}}{l!} \frac{\partial^l}{\partial t^l} + i\gamma |a_n(z, t)|^2 + i2\gamma \sum_{k \neq n} |a_k(z, t)|^2 \right] a_n(z, t) \quad (2)$$

$$\beta_{n,l} = \left(\frac{d^l}{d\omega^l} \beta(\omega) \right)_{\omega=n\Delta\omega} \quad (3)$$

Throughout this paper, $\beta_{n,l}$ indicates the l^{th} Taylor expansion order of the propagation constant at the central frequency of the n^{th} channel, whereas if β parameters are written with only one subscript, that subscript indexes the Taylor expansion order of the fibre propagation constant at a central wavelength of 1550 nm. The four-wave mixing terms have been dropped from (2) as we assume they are not in general phase matched. This assumption may break down for narrow channel separations below ≈ 15 GHz [25]. A common method of investigating XPM [22, 23] also involves discarding second and third order intra-channel dispersion as a first approximation, i.e. setting $\beta_{n,2} = \beta_{n,3} = 0 \forall n$. Under such conditions, the pulses maintain their shape but propagate at group velocities $v_n = 1/\beta_{n,1}$ particular to each channel. This approximation enables the following analytic solution to (2):

$$a_n(z, t) = a_n(0, t - z\beta_{n,1}) \exp\left[-\frac{\alpha z}{2} + i\beta_{n,0} z + i\theta_n + i\phi_n\right] \quad (4)$$

$$\theta_n(z, t) = \gamma |a_n(0, t - z\beta_{n,1})|^2 (1 - e^{-\alpha z}) / \alpha \quad (5)$$

$$\phi_n(z, t) = 2\gamma \sum_{k \neq n} \int_0^z |a_k(0, t - z\beta_{n,1} + z'\mu_{n,k})|^2 e^{-\alpha z'} dz' \quad (6)$$

where $\mu_{n,k} = \beta_{n,1} - \beta_{k,1}$ is the group velocity mismatch between channels n and k . Samples are taken at the end of the fibre $z = L$, from channel n at the peak of the pulse, i.e. the j^{th} sample is taken at time $t = j\Delta_t + z\beta_{n,1}$, where Δ_t is the sampling period. We do not analytically explore the SPM term in (5) as this is not the primary focus of this paper but we do include SPM effects in some numerical simulations in sections 4 and 5. We are however, interested in calculating the XPM phase noise variance of the n^{th} channel that results from (6). The XPM noise contribution from all other channels to the j^{th} sample in the n^{th} channel, i.e. the phase perturbation of the j^{th} symbol from the coded value, is:

$$\begin{aligned} \phi_{n,j} &= 2\gamma \sum_{k \neq n} \int_0^L |a_k(0, j\Delta_t + z\mu_{n,k})|^2 e^{-\alpha z} dz \\ &= 2\gamma L \sum_{k \neq n} \int_0^1 |a_k(0, j\Delta_t \pm sT_{n,k})|^2 e^{-\alpha Ls} ds \end{aligned} \quad (7)$$

where $s = z/L$ is normalised length, $T_{n,k} = L|\mu_{n,k}|$ is the total walk off time between channels n and k at the fibre length L and $\pm = \text{sign}[\mu_{n,k}]$. The method we use to calculate the variance of (7) is similar to [23] although we introduce notable generalisation in sections 3-5 to include DCFs and OPC. As each channel is uncorrelated, the total variance is the sum of the variance of each of the channels. We break the integral in (7) into integrals over each symbol and approximate the loss term in those individual integrals as a constant. Furthermore, for simplicity we assume the integral encompasses an integer number of symbols, $N_{n,k} = \lfloor T_{n,k}/\Delta_t \rfloor$, with $\lfloor \cdot \rfloor$ being the floor function. Hence, (7) is approximated as:

$$\phi_{n,j} \approx 2\gamma L \sum_{k \neq n} \frac{1}{N_{n,k}} \sum_{m=0}^{N_{n,k}-1} P_{k,j+m} \exp\left[-\frac{m\alpha L}{N_{n,k}}\right], \quad P_{k,j} = \int_{-\frac{1}{2}}^{\frac{1}{2}} |a_k(0, (j+s)\Delta_t)|^2 ds \quad (8)$$

Approximating the integral as a sum enables us to use some known statistical analysis. As $P_{k,j}$ are uncorrelated random variables the variance is the sum of their variances with the weights squared, but as the variance of each symbol is the same $\sigma^2(P_{k,j+m}) = \sigma_P^2$, this factors out from the sum over the squared weights. Note that σ_P^2 is the variance in the average power of each symbol at input, but as the pulses are the same shape we have $\sigma_P^2 = \sigma_c^2 P^2$ where P is the

average power per channel at launch and σ_c^2 is the variance in the *peak* power of the modulation format normalized to have mean peak power of 1. Note that σ_c is only non-zero in amplitude modulated formats, for on-off keying: $\sigma_c^2 = 1/4$, for 16 QAM: $\sigma_c^2 = 8/25$, while for 64 QAM: $\sigma_c^2 = 8/21$. Hence, all other things being equal, the standard deviation of inter-channel XPM is almost 13% larger in 16 QAM than in on-off keying and 23% larger in 64 QAM. The phase noise variance of channel n is thus:

$$\begin{aligned}\sigma^2(\phi_n) &\approx 4 \sigma_c^2 P^2 \gamma^2 L^2 \sum_{k \neq n} \frac{1}{N_{n,k}^2} \sum_{m=0}^{N_{n,k}-1} \exp\left[-\frac{2 m \alpha L}{N_{n,k}}\right] \\ &\approx 4 \sigma_c^2 P^2 \gamma^2 L^2 \sum_{k \neq n} \frac{1}{N_{n,k}} \int_0^1 e^{-2\alpha L s} ds = \sigma_c^2 4 P^2 \gamma^2 L L_{2\alpha} \sum_{k \neq n} \frac{1}{N_{n,k}}\end{aligned}\quad (9)$$

with $L_{2\alpha} = (1 - e^{-2\alpha L})/(2\alpha)$. For large αL , (9) tends to the formula in [23]:

$$\sigma^2(\phi_n) \approx \frac{\sigma_c^2 2 P^2 \gamma^2 L}{\alpha} \sum_{k \neq n} \frac{1}{N_{n,k}} \quad (10)$$

3. XPM noise for SMF plus DCF

In this section we will generalise the analysis of section 2 to describe the case of propagation through SMF followed by amplification (a simple scalar multiplication for our analysis) followed by propagation through a DCF. In this case, the analytic solution given in (4) indicates there would be two contributions to XPM:

$$\begin{aligned}\phi_{n,j} &= \sum_{k \neq n} 2 \gamma_1 \int_0^{L_1} |a_k(0, j\Delta_t + z \mu_{n,k})|^2 e^{-\alpha_1 z} dz + \\ &\sum_{k \neq n} 2 g \gamma_2 \int_{L_1}^{L_1+L_2} |a_k(0, j\Delta_t + z \nu_{n,k} + (\mu_{n,k} - \nu_{n,k}) L_1)|^2 e^{-\alpha_2(z-L_1)} dz\end{aligned}\quad (11)$$

where the indices 1 and 2 on α , γ and L refer to the parameters of the SMF and DCF, respectively, $\mu_{n,k} = \beta_{n,1}^{(1)} - \beta_{k,1}^{(1)}$ and $\nu_{n,k} = \beta_{n,1}^{(2)} - \beta_{k,1}^{(2)}$ are the group velocity mismatches of the SMF and DCF, respectively (superscripts label fibre: SMF=1, DCF=2), and $g = G e^{-\alpha_1 L_1}$ represents the ratio of power into the DCF to SMF with G being the linear amplifier gain prior to the DCF; if $g = 1$ then the amplifier exactly compensates the transmission loss of the SMF. We assume the DCF compensates the dispersion of the SMF, hence $L_1 \mu_{n,k} + L_2 \nu_{n,k} = 0$. After the substitution $z = s L_1$ in the first integral of (11) and $z = (1 - s) L_2 + L_1$ in the second, both integrals can be combined to give:

$$\phi_{n,j} = 2 \sum_{k \neq n} \int_0^1 |a_k(0, j\Delta_t \pm s T_{n,k})|^2 (\gamma_1 L_1 e^{-\alpha_1 L_1 s} + g \gamma_2 L_2 e^{\alpha_2 L_2 (s-1)}) ds \quad (12)$$

where $T_{n,k} = L_1 |\mu_{n,k}| = L_2 |\nu_{n,k}|$, $\pm = \text{sign}[\mu_{n,k}]$. This reverse of the DCF power profile with respect to the time variable (i.e. $1 - s$) is not just a mathematical trick, crucially it indicates that the power profile as a function of the channel temporal separation actually possesses some amount of symmetry when a SMF is followed by a DCF designed to fully compensate the SMF dispersion, provided both fibres have positive loss coefficients, as naturally they would. Generally, the symmetry is not exact due to differences in the material properties of the SMF and DCF and the significance of this in the context of OPC will be discussed further in sections 4 and 5. Following similar analysis to section 2, the variance of (12) is approximately:

$$\sigma^2(\phi_n) \approx 4 \sigma_c^2 \sum_{k \neq n} \frac{1}{N_{n,k}^2} \sum_{m=0}^{N_{n,k}-1} y^2\left(g, \frac{m}{N_{n,k}}\right) \approx 4 \sigma_c^2 \int_0^1 y^2(g, s) ds \sum_{n \neq k} \frac{1}{N_{n,k}} \quad (13)$$

$$y(g, s) = R_1 e^{-\alpha_1 L_1 s} + g R_2 e^{\alpha_2 L_2 (s-1)}, \quad R_i = P \gamma_i L_i \quad (14)$$

where $y(g, s)$ is referred to hereafter as the normalised nonlinear profile and P is the average channel power at the very start of the link. The integral in (13) is easily evaluated and this completes the generalization of the phase noise model of [23] to include the use of DCFs. (13) is quite intuitive, the factor 4 is the square of the 2 typically associated with XPM effects and the other three dimensionless factors that appear are: a term related to the modulation format peak power variance, an integrated normalised nonlinear profile and a sum which reduces with increased dispersion. The true novelty of our work will follow in sections 4 and 5 where we will include OPC. Finally, it is to be noted that, in this model if M_{sp} spans of consecutive SMF+DCF blocks were put together back to back, with the same fibre properties and with the same SMF to DCF input power ratio in each block, then $\sigma(\phi_n)$ would simply scale to $M_{sp} \sigma(\phi_n)$.

4. XPM noise with OPC: case 1

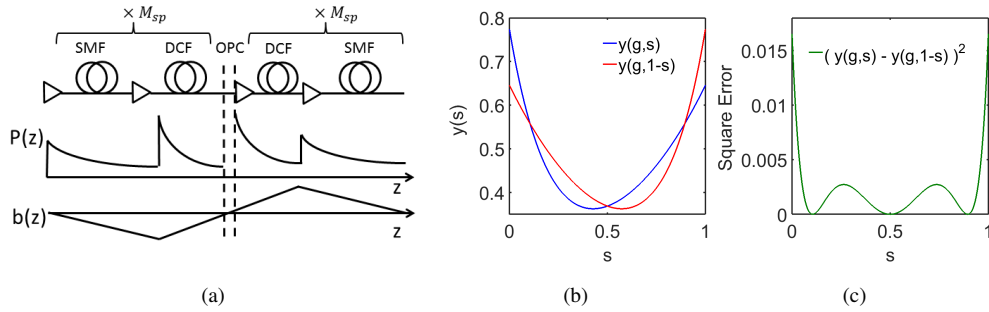


Fig. 1. a) Fibre setup, power $P(z)$ and accumulated dispersion $b(z)$, b) nonlinearity profiles with $g = g_{opt} = 1.34$ (Blue: pre-OPC, Red: post-OPC), c) their square error.

This section and section 5 contain the main objective of the paper, the generalization of the inter-channel XPM phase noise analysis to include OPC. Consider the setup SMF→DCF→OPC→DCF→SMF, shown in the first row of Fig 1a. Here, amplifiers are placed before every fibre so that the power profile will rise and fall as indicated in the second row of Fig 1a. We assume both SMFs are the same and that the launch powers into them are the same, likewise, both DCFs are the same and that the launch powers into them are the same, with g parametrizing the launch power into the DCF relative to the SMF. The DCF is fully compensating so the accumulated dispersion $b(z) = \int_0^z \beta_2(z') z' dz'$ (where $\beta_2(z)$ is a different constant in the SMFs and DCFs) will increase then return to zero as indicated in the third row of Fig 1a. The conjugation will introduce a minus sign in front of the XPM phase integral in (12) corresponding to pre OPC propagation. The noise from XPM incurred prior to the OPC can thus be cancelled by a similar integral associated with post OPC propagation provided that the two contributions are correlated. To achieve correlation, two things need to happen. First, because the OPC will introduce spectral inversion, the channels will change frequency and hence group velocity. If the inversion is about the central wavelength of an approximately symmetric dispersion profile ($\beta_3 \approx 0$) then the sign of the relative propagation constants will be reversed but the magnitudes will be roughly comparable. To correct for the change in sign of the group velocity mismatch, it is thus necessary to reverse the order of the DCF and SMF in any post OPC span relative to the corresponding pre OPC fibre pair. This ensures that the set of pulses swept by the XPM integral are the same in each case (correlated in time). The second thing that needs to happen is that

the weight of each pulse being swept in the integral, i.e. the value of the nonlinearity profile associated with a pulse in a neighbouring channel at the instant it passes a pulse in the channel of interest, is similar in both pre and post OPC propagation so as to cancel when subtracted. In this current scenario, Case 1, because the order of the SMF and DCF fibres is reversed post OPC but the fibres of the same type share the same input powers, the post OPC nonlinear profile $y(g, 1 - s)$, where s is a normalised fibre length variable, is equal to the pre-OPC nonlinear profile $y(g, s)$ reflected about $s = 1/2$, where $y(g, s)$ is defined in (14). Put more simply, in this arrangement of power levels and amplifiers, reversing the order of the fibres reverses the nonlinear profile. Both nonlinear profiles are plotted in Fig 1b. The difference between these curves will be minimized when the curve is symmetric about $s = 1/2$. As noted in section 3, in reality the SMF and DCF will have different material properties and thus the symmetry will not be exact but, crucially, the curve can be made more symmetric by tuning g , the input power ratio of the SMFs to DCFs. Subtracting the two profiles then gives an effective nonlinear profile for the entire system and squaring the result gives the *square error* of the curves and is plotted in Fig 1c. Following the logic of section 3, the total channel phase noise variance for the set-up in Fig 1a is proportional to the *integrated square error* between the curves. More explicitly:

$$\sigma^2(\phi_n) \approx 4 M_{sp}^2 \sigma_c^2 \int_0^1 [y(g, s) - y(g, 1 - s)]^2 ds \sum_{n \neq k} \frac{1}{N_{n,k}} \quad (15)$$

In deriving (15), we have ignored the fact that there may be some small difference in $N_{n,k}$ before and after the OPC due to small asymmetry in the dispersion profile ($\beta_3 \neq 0$) as this allows us to factor out $1/N_{n,k}$ and minimize all channels simultaneously. The integral in (15) will not vanish exactly as dispersion compensating fibres are typically much shorter in length and have larger nonlinear coefficients and loss than the SMF, thus there will be residual asymmetry. On inspection of (14), there would be an exact solution if $\alpha_1 L_1 = \alpha_2 L_2$, which demands that the ratio of fibre material properties $\alpha_i/\beta_2^{(i)}$ takes the same value in each fibre as the fibre lengths are already related through dispersion compensation. In this case, one would set $g = \gamma_1 L_1 / (\gamma_2 L_2)$ to balance the nonlinear lengths. However, while there may be some limited scope for tuning the design of the DCF, the most obvious parameter for minimizing the integral in (15), and thus the residual phase noise, is g , i.e. the launch power into the DCF. The integral in (15) is easily evaluated, giving a quadratic in g which is minimized at the optimal g value g_{opt} such that:

$$\int_0^1 [y(g_{opt}, s) - y(g_{opt}, 1 - s)]^2 ds = \left(\frac{4 C_1 S_1}{l_1} - 2 \right) R_1^2 e^{-l_1} - \left(\frac{4 C_2 S_2}{l_2} - 2 \right) g_{opt}^2 R_2^2 e^{-l_2} \quad (16)$$

$$g_{opt} = 4 \frac{\alpha_2 \gamma_1 l_1 (C_1 S_2 l_1 - C_2 S_1 l_2)}{\alpha_1 \gamma_2 (l_1^2 - l_2^2) (2 C_2 S_2 - l_2)} \exp \left[-\frac{(l_1 - l_2)}{2} \right] \quad (17)$$

where $l_i = L_i \alpha_i$, $C_i = \cosh(l_i/2)$ and $S_i = \sinh(l_i/2)$. This optimization is dependant on the fibre properties and amplifier power ratios but not on the data properties.

As an example, we consider 5×16 -QAM WDM channels, each with a symbol rate of 13.3 Gbaud. The pulses were super-Gaussian with a $1/5$ duty-cycle. The other data parameters were: $\Delta_t = 75$ ps, $\Delta\omega = 2\pi \times 110$ GHz, $\sigma_c^2 = 8/25$ and $P = 6.3$ mW. The SMF parameters were: $M_{sp} = 1$, $\gamma_1 = 1$ /W/km, $\alpha_1 = 0.2$ dB/km, $L_1 = 100$ km, $\beta_2^{(1)} = -0.0210$ ps²/m, $\beta_3^{(1)} = -9.42 \times 10^{-5}$ ps³/m. The DCF parameters were: $\gamma_2 = 7.6$ /W/km, $\alpha_2 = 0.64$ dB/km, $L_2 = 10$ km, while the DCF dispersion parameters were $\beta_2^{(2)} = -\beta_2^{(1)} L_2/L_1$, $\beta_3^{(2)} = -\beta_3^{(1)} L_2/L_1$. These parameters were based on standard fibres available in the market. For the OPC, we take the complex conjugate of the total electric field which introduces spectral inversion, we do not simulate the conjugating FWM process as this is not our focus but it would typically involve

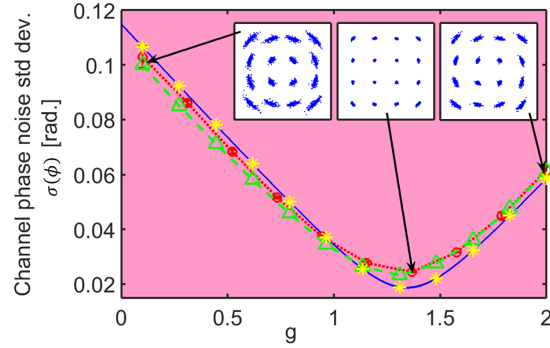


Fig. 2. XPM noise standard deviation as a function of DCF/SMF power ratio, g , Case 1. Blue-solid: analytic, (15). Yellow-stars: numeric (2), $\beta_{2,n} = \beta_{3,n} = 0$. Green-dashed-triangles: numeric (2), $\beta_{2,n} \neq 0$, $\beta_{3,n} \neq 0$. Red-dotted-circles: numeric (1). Inset: 16-QAM output constellations at low, optimal and high g , numeric, (1).

mixing the signal channels with a strong pump beam in a highly nonlinear fibre to generate their conjugate as an idler field [11]. To calculate phase noise in the numerical simulations, we first digitally correct the mean phase rotation of each amplitude level of the modulation format due to the SPM term in (5) and then calculate the variance of the remaining phase noise of all samples explicitly. The numerical simulations use the split-step Fourier method and take the mean of 5 identical simulations which differ only in the initial random symbol value assignment. Fig. 2 shows the phase noise standard deviation for one channel $\sigma(\phi)$ (mean of all channels) as g is varied. The solid blue line is our analytic model, (15), while the yellow stars show a numerical solution of (2) with $\beta_{n,2}^{(i)} = \beta_{n,3}^{(i)} = 0 \forall n$. As expected, their very good agreement confirms that the analytic formulas do indeed model phase noise when there is no intra-channel dispersion and no inter-channel FWM. In this case, the noise is minimised when $g = g_{opt} = 1.34$ as predicted by (17). The green dashed line with triangles is a numerical simulation of the channel model (2) with $\beta_{2,n}$ and $\beta_{3,n}$ given by (3), so it includes intra-channel dispersion and the pulses will broaden in the SMF and shorten again in the DCF with intra-channel inter-symbol nonlinear effects occurring in between. These effects modify the curve from (15), although not by a significant amount so as to invalidate the dominance of the inter-channel XPM, or shift the optimal g value. Finally, the red dotted line with circles shows a numeric simulation of the field model in (1), which includes all dispersive and nonlinear effects, including inter-channel FWM. This is the most realistic model but it can be seen that, with the parameters used, there is not a significant difference to the channel model because inter-channel FWM is not significant. The insets of Fig. 2 show the complex electric field constellation diagrams at the output of the link for low, optimal and high values of g obtained numerically using the field model in (1). At low and high g there is considerable phase noise but for the optimal g value the signal quality is very good. The red dotted line with circles in Fig. 2 also shows that the phase noise in the numeric simulation at $g = 1$ is $\sigma(\phi) = 0.035$, while at optimal $g = 1.34$ it is $\sigma(\phi) = 0.025$. Consequently phase noise is reduced by about 30% by the optimization process compared to the situation where the power launched into all SMFs and DCFs is the same. The model suggests that a similar improvement would also manifest at higher powers or with more repeated SMF-DCF pairs. We return to compare these different values for g in a bit error rate (BER) simulation in section 6 using 64-QAM.

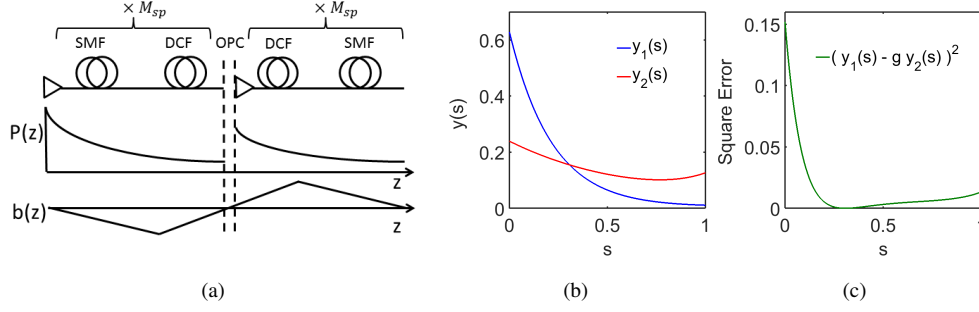


Fig. 3. a) Fibre setup, power $P(z)$ and accumulated dispersion $b(z)$, b) nonlinearity profiles with $g' = g'_{opt} = 0.5$ (Blue: pre-OPC, Red: post-OPC), c) their square error.

5. XPM noise with OPC: case 2

For comparison, we discuss Case 2 with no amplifiers between fibres either side of the OPC but amplifiers at the beginning of each fibre pair so power drops continuously in each half of the link as indicated in Fig. 3a. The fibres are the same as Case 1, section 4, but Case 2 has the advantage of using half the number of amplifiers. This time, we optimize the system by tuning the ratio of power into the link after the OPC relative to the initial input power at the start of the link, g' , so as to minimize asymmetry in the nonlinear profile either side of the OPC. It can be shown by following similar analysis as that presented in section 3 and 4 but modified to accommodate the different amplifier arrangement, that the XPM phase noise variance for Case 2 is:

$$\sigma^2(\phi_n) \approx 4 M_{sp}^2 \sigma_c^2 \int_0^1 [y_1(s) - g' y_2(s)]^2 ds \sum_{n \neq k} \frac{1}{N_{n,k}} \quad (18)$$

$$\begin{aligned} y_1(s) &= R_1 \exp[-\alpha_1 L_1 s] + R_2 \exp[\alpha_2 L_2 (s-1) - \alpha_1 L_1] \\ y_2(s) &= R_2 \exp[-\alpha_2 L_2 s] + R_1 \exp[\alpha_1 L_1 (s-1) - \alpha_2 L_2] \end{aligned} \quad (19)$$

where y_1 and y_2 are the normalised nonlinear profiles of the link before and after the OPC, respectively. To calculate phase noise in the numerical simulations, we first digitally correct the mean phase rotation of each amplitude level of the modulation format due to the SPM term in (5) and then calculate the variance of the remaining input-output phase difference of all samples explicitly. Fig. 4 shows the analytic and numeric results from the Case 2 example. The launch power at the start was the same as the Case 1 example, as were all the fibre and data related parameters. The only difference is the amplifier arrangement. If $g' = 1$ then the amplifier after the OPC compensates the loss of the link prior to the OPC and the launch power after the OPC matches the launch power at the start of the link. The solid blue line is our analytic model of the XPM noise standard deviation, the square root of (18), while the yellow stars are a numerical solution of (2) with $\beta_{2,n} = \beta_{3,n} = 0$. Again, as expected, these two curves are in very good agreement confirming our analytic formulas model phase noise when there is no intra-channel dispersion and no inter-channel FWM. The noise is minimised when $g' = g'_{opt} = 0.5$ as predicted by a minimization of the integral in (18). The green dashed line with triangles is a numerical simulation of the channel model (2) with $\beta_{2,n}$ and $\beta_{3,n}$ given by (3), this includes intra-channel dispersion and the pulses will broaden in the SMF and shorten again in the DCF, with intra-channel inter-symbol nonlinear effects occurring in between. These effects modify the curve from (18), although not by a significant amount so as to invalidate the dominance of the inter-channel XPM, or shift the optimal g' value. Finally, the red dotted line with circles shows

a numeric simulation of the field model in (1), which also includes inter-channel four-wave mixing. With the parameters used there is good agreement between the simple analytic model and the field model below $g' = 0.5$ and although there is some divergence at larger g' the simple analytic model still indicates that inter-channel XPM accounts for more than 80% of all phase noise. For the parameters used, inter-channel XPM is well-modelled by our analysis and can be significantly minimised by an appropriate tuning of the power into the link after the OPC. Crucially though, we observe that at optimized power settings, the minimal phase noise is 50% larger for Case 2, than for Case 1 as there is more asymmetry in the nonlinear profiles of Case 2 due to the absence of amplifiers between fibres either side of the OPC.

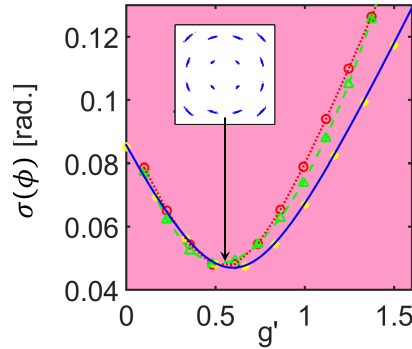


Fig. 4. XPM noise standard deviation as a function of pre/post-OPC power ratio, g' , Case 2. Blue-solid: analytic (18). Yellow-stars: numeric (2), $\beta_{2,n} = \beta_{3,n} = 0$. Green-dashed-triangles: numeric (2), $\beta_{2,n} \neq 0$, $\beta_{3,n} \neq 0$. Red-dotted-circles: numeric (1). Inset: 16-QAM constellation at optimal g' , numeric (1).

6. Bit error rate test with 64-QAM

In this section we perform a BER simulation to demonstrate the improvement provided by optimising the DCF/SMF input power ratio via our method. We take the amplifier arrangement in Fig. 1a with $M_{sp} = 2$. In this instance we use Gray coded 64-QAM data. The pulses were super-Gaussian with a 0.48 duty-cycle and the symbol rate was 17 Gbaud. The other data parameters were: $\Delta_t = 58\text{ps}$, $\Delta\omega = 2\pi \times 66\text{GHz}$ but all other fibre parameters are the same as Section 4. We use 64-QAM data here rather than 16-QAM as it encounters errors at shorter distances for the same power levels as 16-QAM and this allows us to shorten the simulation time. However, changing modulation format also allows us to demonstrate that our optimization process works just as well for all amplitude modulation formats. In this section we add spontaneous emission noise in our simulation of the amplifiers to investigate operation in a realistic scenario. This is done by adding a noise vector at every amplifier such that the noise figure is always 4 dB. We also add a noise vector at the input that is held at a constant value such that if we increase the average input power the input optical signal to noise ratio improves. The input noise level was set at an arbitrary level such that at 0 dBm the input optical signal to noise ratio (OSNR) was 40 dB. In Fig 5 the blue circles show the BER at the end of the link when $g = 1$ which means the power launched into all the DCFs is the same as that launched into the SMFs, while the red squares show the BER when the system is optimized using the method devised in Section 4 such that $g = 1.34$. In all Fig.s there is a minimal BER as the system is limited by amplifier noise at low power and nonlinear noise at high power. In Fig 5a, Fig 5b and Fig 5b we use 7, 13 and 25 frequency channels, respectively and our optimization process can be seen to reduce the minimal BER by 83%, 78% and 54%, respectively. The BER improvement through optimization reduces as the channel number increases due to four-wave mixing which increases with channel number

but is not as well compensated as the inter-channel XPM and thus the additional power in the DCF when $g = 1.34$ rather than $g = 1$ creates additional four-wave mixing noise which off-sets the optimization process to some extent, although the improvement is still significant.

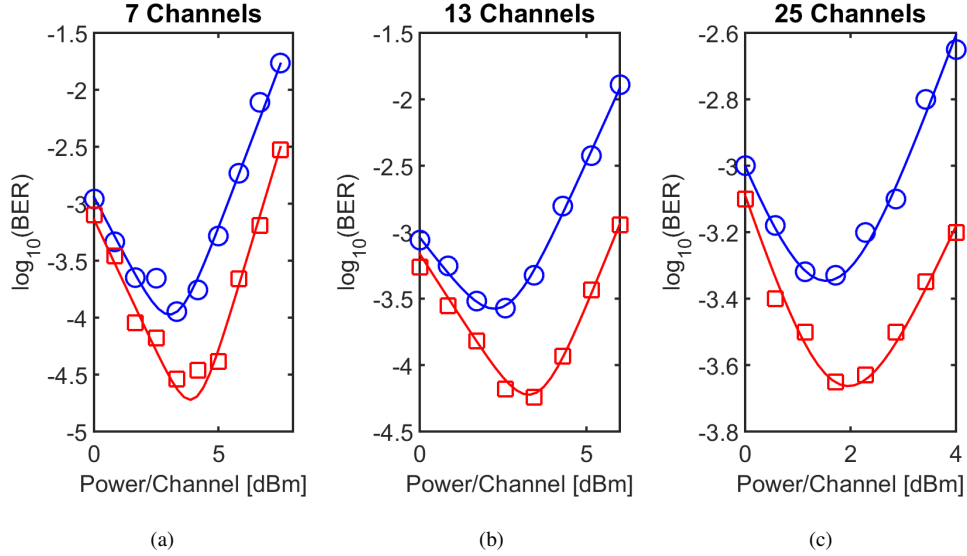


Fig. 5. BER as a function of input average power P for two amplifier settings, $g = 1$ (blue circles) and optimized $g = 1.34$ (red squares) for a) 7 channels b) 13 channels c) 25 channels.

7. Conclusion

We studied asymmetric nonlinear profiles in fibre transmission paths about an optical phase conjugator using analytic and numerical modelling in dispersion managed fibre links. We showed, that inter-channel XPM noise is proportional to the integrated square error between nonlinear profiles either side of the OPC and can be significantly reduced by tuning power levels in a simple arrangement of amplifiers, even for non-ideal fibre parameter scaling laws.

Funding

This work was funded in part by the EPSRC grant EP/I01196X, The Photonics Hyperhighway and in part by the EPSRC Doctoral Prize EP/M50662X/1 awarded to Dr Graham Hesketh.